[1]YuYing Wang[1*]
Min Ding[1]
Jun Tin Li[1]
Rong Fa Chen[1]
Wen Zhe Mei[1]

Research on Online Partial Discharge Detection Technology of Underground Power Distribution Cabinets Based on Capacitive Insulator Coupling

Journal of Electrical Systems

Abstract: - Aiming to address the susceptibility of existing capacitive insulator coupling technology to ground grid interference in partial discharge (PD) monitoring for underground distribution cabinets, and its unreliable performance in humid environments, this paper proposes a real-time wireless PD monitoring method us-ing capacitive insulator coupling. By analyzing the response characteristics of coupled signals from dis-charge defects, a simulation model for signal propagation and ground interference was developed and validated on an experimental platform. Results show: 1) The model accurately simulates air-gap dis-charge mechanisms and signal propagation, aligning with experimental time-domain responses; 2) Ground grid interference propagates via common-ground impedance wide-frequency coupling, and the "common grounding point" method effectively suppresses it, significantly improving the signal-to-noise ratio; 3) Phase-resolved PD patterns exhibit typical "bimodal" features, consistent with the simulated in-ternal air-gap discharge model, verifying the system's capability to identify typical insulation defects. This study offers theoretical and practical insights for optimizing capacitive coupling technology and enabling high-sensitivity PD detection in complex environments.

Keywords: Partial Discharge (PD); Capacitive Insulator Coupling; Propagation Characteristics; Ground Grid Inter-ference; Phase-Resolved Partial Discharge (PRPD) Pattern.

1. Introduction

Underground power distribution rooms are an indis-pensable part of the modern urban power supply system, and their safe and stable operation has a bearing on the power supply of the entire city [1,2]. Due to the humid and high-temperature underground environment, power equip-ment enclosed in underground switchgear will develop insu-lation defects during long-term operation, leading to the occurrence of partial discharge (PD) [3,4]. PD is an im-portant manifestation of insulation defects in switchgear. In severe cases, it may even lead to fires or explosions, threat-ening the safe operation of the power grid. Therefore, strength-ening PD detection and accurately locating the discharge source is crucial for the safe operation of power distribution cabinets [5,6].

When partial discharge occurs inside the switchgear, it is usually accompanied by acoustic, optical, electrical and vibration phenomena [7,8], Currently, partial discharge de-tection primarily falls into two major categories: non-electrical measurement methods and electrical meas-urement methods [9]. Among these electrical testing meth-ods, the primary ones include the pulse current method, the Ultra High Frequency (UHF) method, and the Transient Earth Voltage (TEV) method [10,11]; Non-electrical meas-urement methods primarily include optical measurement and ultrasonic methods [12,13]. For switchgear, the chal-lenge lies in online monitoring during live operation, which is also a crucial means for obtaining real-time insights into switchgear health status and identifying potential safety hazards [14]. To address partial discharge (PD) issues in dis-tribution switchgear, researchers have proposed various monitoring techniques. Reference [15] proposes an inte-grated passive wireless temperature and partial discharge monitoring method for high-voltage switchgear. Utilizing RF energy harvesting and backscatter communication tech-nology, it integrates ultra-high-frequency sensing with sur-face acoustic wave temperature sensing into a single node. By separating and acquiring real-time partial discharge and temperature data, it enables comprehensive monitoring of switchgear operational status. Reference [16] introduces an innovative switchgear fault diagnosis technique. Different fault types produce distinct gas compositions. By analyzing characteristic gas components generated during partial dis-charges, this method enables equipment condition assess-ment. Reference [17] proposes a partial discharge fault di-agnosis method for distribution switchgear based on a glob-al feature-enhanced residual contraction network. This ap-proach adaptively suppresses noise and extracts discrimina-tive features from noisy partial discharge signals, achieving excellent recognition accuracy under strong noise interfer-ence. However, these methods have inherent limitations. Underground distribution cabinets typically operate in envi-ronments with ground grid interference and high tempera-tures/humidity, rendering existing approaches unreliable for underground applications and quantitative assessment of discharge defect severity [18,19].

[1] State Grid Suzhou Power Supply Company, China.
[*] Corresponding author: jsdky2026@163.com

Based on this, this paper proposes a real-time wireless PD monitoring technology based on capacitive insulator coupling, capable of reliably detecting and quantitatively assessing the severity of discharge defects. By analyzing the propagation characteristics of coupled signals from dis-charge insulation defects in underground substations, an experimental platform simulating electrical signal propaga-tion in underground substations was established, and its simulation model was constructed using SIMULINK. Ex-perimental and simulation studies reveal the propagation patterns of coupling signals from discharge insulation de-fects and ground network interference signals in under-ground substations, validating the effectiveness and reliabil-ity of the proposed method..

2. Simulation Study on Signal Propagation in Underground Electrical Distribution Rooms

To investigate the propagation characteristics of PD coupling signals and ground network interference signals in underground substations, this section will establish a propa-gation simulation model. The core of the monitoring meth-od proposed in this study lies in utilizing capacitive insulator coupling sensing technology, a typical implementation method for live display device coupling. Its working princi-ple is as follows: the capacitive insulators used for mechan-ical support and electrical insulation in switchgear are sim-ultaneously employed as high-frequency current sensors. When partial discharge occurs within the cabinet, the result-ing steep pulse current couples to the grounding wire through the equipment's stray capacitance. By connecting a high-frequency detection impedance in series with the grounded end of the capacitive insulator, the PD-coupled signal flowing through can be captured. This method elimi-nates the need for additional sensors on the high-voltage side, enabling non-intrusive measurement. It is particularly suitable for online monitoring in compact, space-constrained underground distribution cabinets. Based on this sensing principle, the equivalent circuit model for PD coupling signal propagation is shown in Figure 1. This model utilizes capacitor insulators as coupling elements to non-invasively introduce high-voltage PD pulses into the detection circuit. Subsequent sections will establish propaga-tion simulation models for both PD coupling signals and interference signals to conduct in-depth analysis of their characteristics.

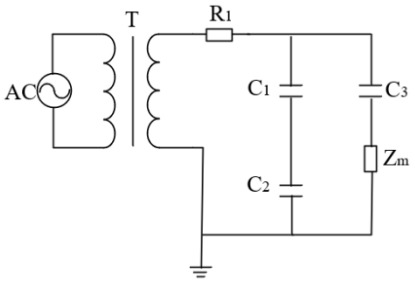

Fig. 1. Equivalent Circuit Model for PD-Coupled Signal Propagation

2.1 PD-Coupled Signal Propagation Simulation

Using SIMULINK software for simulation research on PD-coupled signal propagation, an equivalent circuit model as shown in Figure 2 was established.

Simultaneously, to reduce complexity and facilitate subsequent analysis, circuit models for detection impedance, PD defects, and other components were encapsulated based on a modular approach, forming corresponding subsystems. The specific structures of each subsystem are as follows:

1) Detection Impedance Subsystem

The detection impedance subsystem employs an RLC-type detection impedance. The voltage across its ter-minals is measured by a voltage measurement element and transmitted to the oscilloscope on the main interface via a Goto element. The detailed structure of the detection im-pedance subsystem is shown in Figure 3.

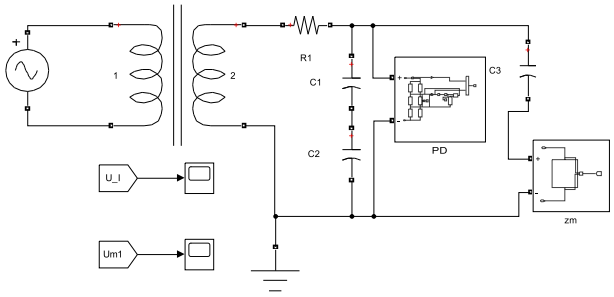

Fig. 2. SIMULINK Simulation Circuit Model

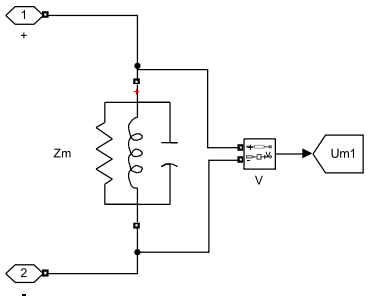

Fig. 3. Detection Impedance Subsystem

2) Typical PD Fault Simulation Subsystem

For PD simulation, an equivalent model is established targeting typical PD phenomena occurring in the presence of air gaps. When air gaps exist within solid or liquid insulating media, they can be approximated using the circuit model shown in Figure 4. Among these,Cg represents the capaci-tance of this air gap. Cb1 and Cb2 represent the capacitance of the portion of the dielectric material connected in series with the air gap, while Ca represents the capacitance of the remaining intact portion of the dielectric material. When the voltage across the air gap rises to the gap's breakdown volt-age, discharge occurs within the gap. The charges on both sides of capacitor Cg are released through the discharge, causing the voltage to rapidly drop to the extinction voltage, whereupon the discharge ceases [20,21]. As the applied voltage continues to rise, Cg recharges until the voltage across its terminals again reaches the discharge voltage, triggering a second discharge. Similarly, Rg, Rb1 and Rb2 rep-resent the insulation resistance of the air gap and the re-sistance of the two insulation materials connected in series with the air gap, respectively. Under normal conditions, Rg, Rb1 and Rb2 are all at relatively high levels, with their im-pedance values far exceeding the capacitive impedance in parallel. Therefore, the voltage division in the series branch is primarily determined by the three capacitors.

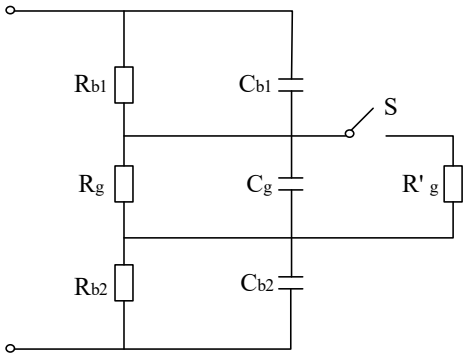

Fig. 4. Circuit Model of Air Gap Discharge

Based on the circuit in Figure 4, the charge released during each air gap discharge can be derived as:

$$q_r \approx (C_g + \frac{C_{b1}C_{b2}}{C_{b1}+C_{b2}}) \cdot (U_{on} - U_{off}) \quad (1)$$

Simultaneously, a corresponding PD simulation sub-system was constructed in SIMULINK, as shown in Figure 5. First, the voltage measurement module measures the volt-age across the air gap capacitor Cg. The Absolute Value Module (Abs) then extracts the absolute value of this volt-age. Based on this absolute value, the Delay Module (Relay) generates high and low logic levels to control the switch's on/off state, thereby controlling the PD: When the absolute value of the air gap voltage reaches the initial discharge voltage, the Relay outputs a high logic level. When control switch S1 closes, the air gap discharges through the resistor, causing the voltage to drop. When the absolute value of the air gap voltage falls below the discharge voltage, the relay outputs a low level. Control switch S1 is open, and discharge has stopped. For easier observation. For ease of observation, measure the voltage on both sides of Cg and the total circuit current, then transmit these readings via the Goto compo-nent to the main circuit interface for oscilloscope output.

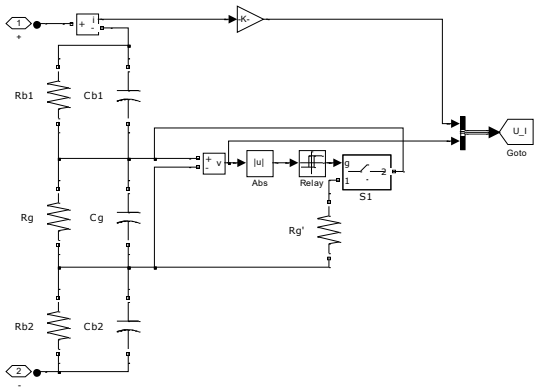

Fig. 5. PD Analog Subsystem

The main parameter settings for the PD simulation subsystem are as follows: Cg = 0.174 pF, Cb1 = Cb2 = 0.348 pF, Uon=4000 V, Uoff= 1400 V. Running the simulation yields the voltage waveforms across both ends of the air gap and the detection impedance, as shown in Figure 6. The figure indicates that the pulse current signal amplitude at this point is 20 mV.

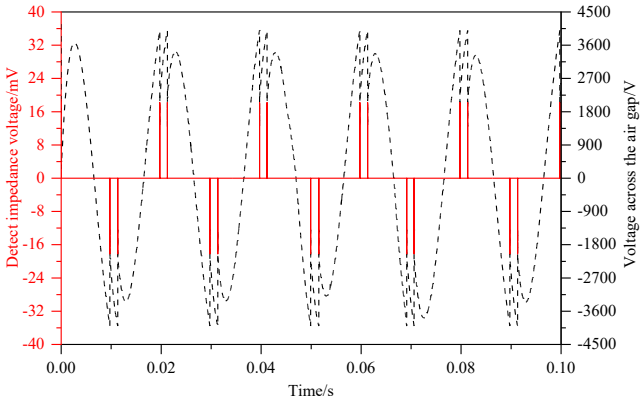

Fig. 6. PD Simulation Results

2.2 Ground Grid Interference Signal Propagation Simulation

To analyze the propagation characteristics of interfer-ence signals, a Gaussian white noise interference signal source was constructed using a Random Number module and a controlled voltage source, as shown in Figure 7. Its current waveform and corresponding FFT analysis results are presented in Figure 8.

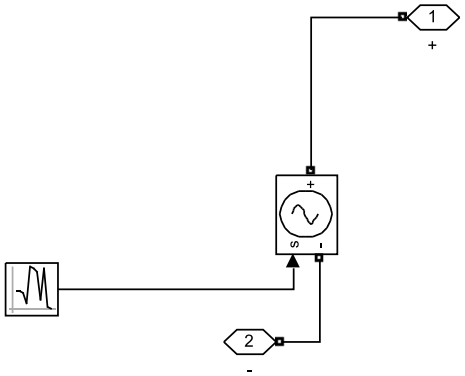

Fig. 7. Gaussian White Noise Disturbance Source Model

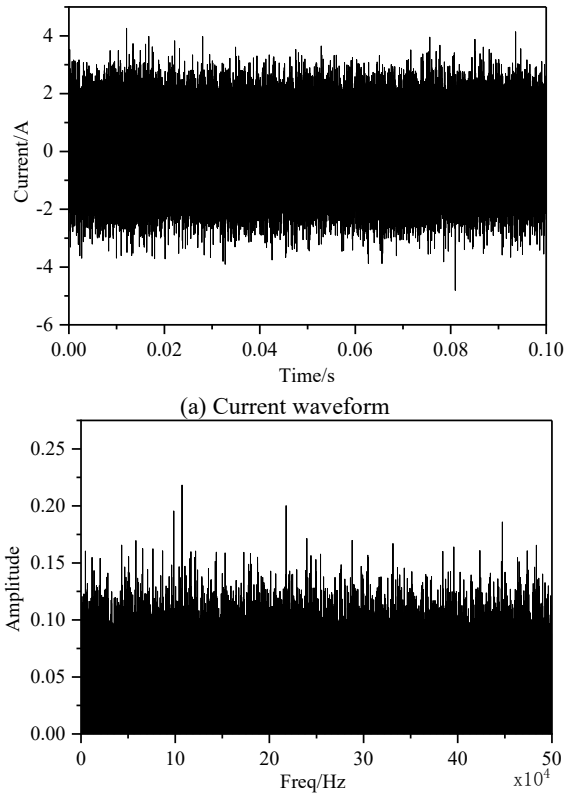

(a) Current waveform

(b) FFT analysis results

Fig. 8. Current Waveform of the Interference Source and FFT Analysis Results

To analyze the propagation characteristics of interfer-ence signals when the interference source is located on the grounding grid side, the interference source in Figure 7 is connected in series between the grounding terminal of the distribution cabinet and the grounding grid. When each de-vice is individually grounded, the SIMULINK simulation circuit model is shown in Figure 9.

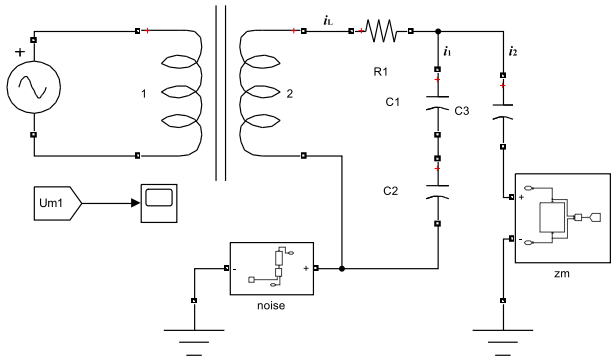

Fig. 9. Simulation Model for Individual Grounding of Each Device

The current waveforms of each branch circuit and their corresponding FFT analysis results are shown in Figures 10-12 below.

Simulation results indicate that when Gaussian-like white noise interference exists on the local network side and the detection system employs an independent grounding method, this interference signal can effectively couple to each measurement branch through the common ground impedance path. The frequency domain analysis of branch currents i1 and i2 clearly indicates that the interference en-ergy is widely distributed across the frequency spectrum.

When multiple devices share the same grounding point, the simulation model is shown in Figure 13. At this point, the interference signal has no path to flow, resulting in zero branch currents. This demonstrates that during PD detection, having all devices share a common grounding point is the most effective measure for suppressing interference signals on the grounding network side.

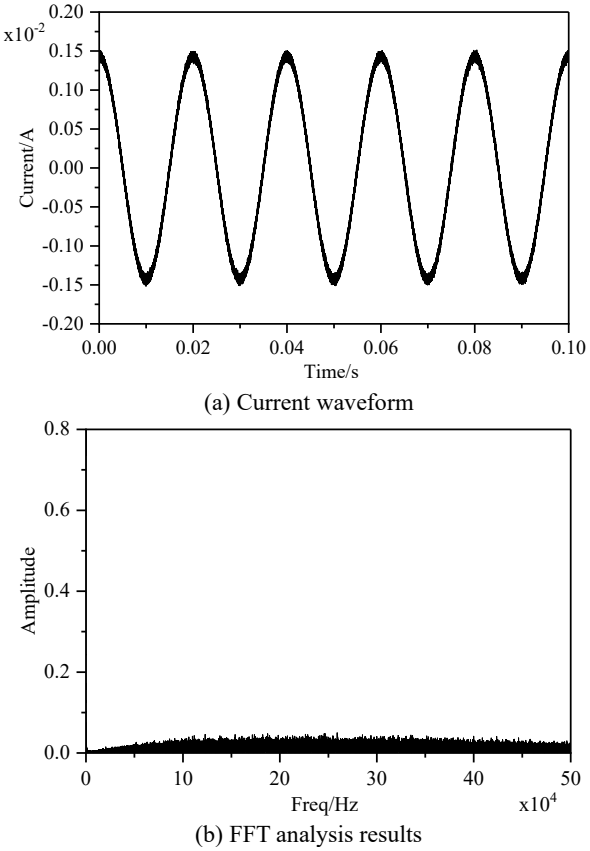

Fig. 10. Current Waveform and FFT Analysis Results of i_L

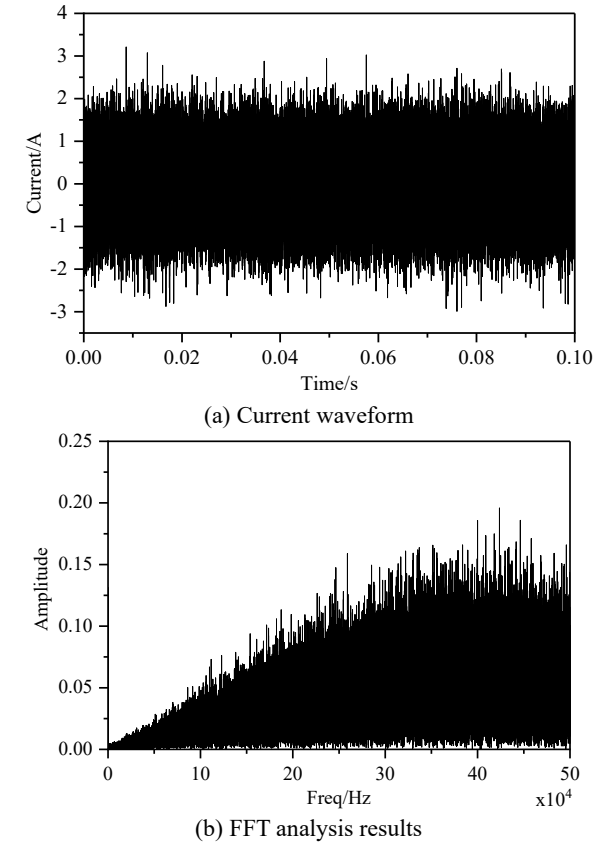

Fig. 11. Current Waveform and FFT Analysis Results of i_1

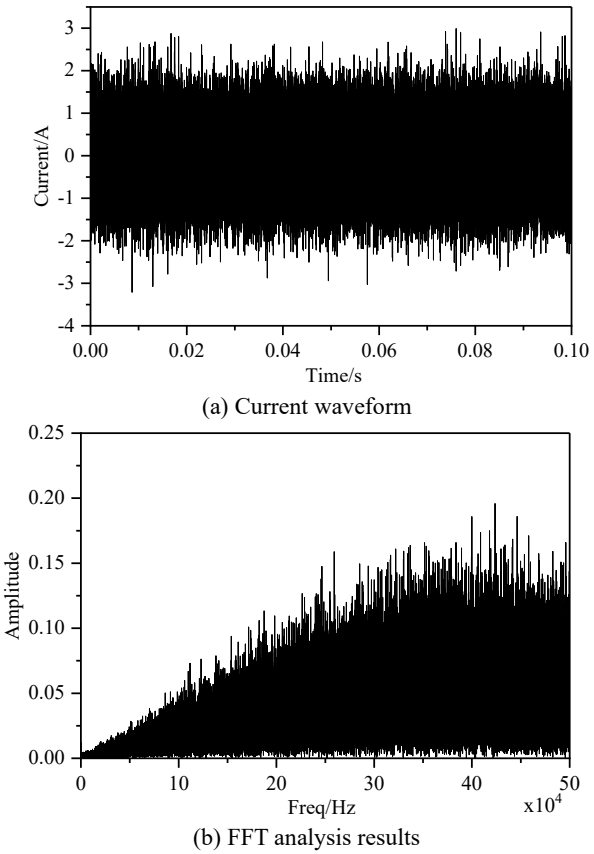

(a) Current waveform

(b) FFT analysis results

Fig. 12. Current Waveform and FFT Analysis Results of i_2

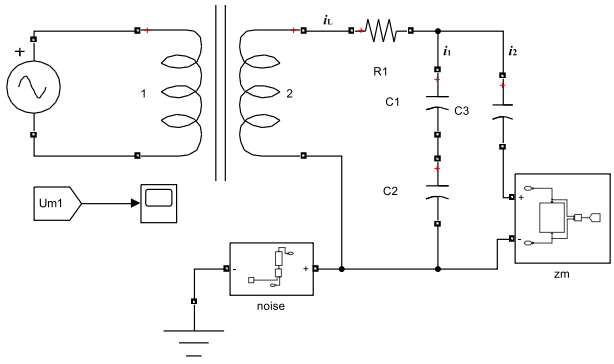

Fig. 13. Simulation Model for Equipment Sharing a Common Grounding Point

3. PD Experimental Platform Setup and Testing Validation

3.1 Experimental Platform Setup

The experimental platform in this paper establishes a PD detection circuit with a series connection of coupling capacitor C3 (capacitor insulator) and detection impedance Z, in accordance with IEC 60270[22] and GB/T 7354 stand-ards [23]. The experimental switchgear utilizes a 10 kV Schneider SM6 ring main unit, with the wiring diagram shown in Figure 14. Among these, C1 and C2 are volt-age-dividing capacitors. The high-voltage capacitor C1 has a value of 413.7 pF, while the low-voltage capacitor C2 has a value of 413.3 nF, The voltage-dividing ratio is 1000:1. The power frequency periodic signal is transmitted from C2 to the Tektronix high-performance digital oscilloscope via a coaxial cable.C3 has a capacitance value of 42pF,T1 is a voltage regulator,T2 is a transformer with a turns ratio of 250:1,R1 serves as a protective resistor. Additionally, to sim-ulate the humid conditions of an actual underground distri-bution room (where moisture originates from both ambient humidity and damp air within the indoor trenches), the trenches connect to the switchgear cable compartments. Due to the need for cable routing

between these areas, both locations exhibit relatively poor sealing integrity[24,25], In some cases, switchgear cable compartments are directly connected to indoor trenches, allowing moist air from the trenches to enter the cable compartments in large quantities and resulting in elevated relative humidity within these areas [26,27]. Although each compartment of the switchgear is separated, connections between compartments still exist due to wiring and other factors, enabling moist air from the cable compartments to infiltrate other compartments as well [28,29]. Poor sealing of switchgear cabinets within sub-stations allows moist air and dust to enter the enclosures. Accumulated dust reduces creepage distances for compo-nents like surge arresters, posing significant safety hazards to equipment operation [30,31], This paper describes the design of a humidity control system for an experimental chamber within a laboratory circuit. The system comprises an acrylic shell, PD defect, conductive rod, ventilation holes, LY-A1 smart humidifier (capable of setting humidity values from 1-99% RH), and Delixi DM-1070 handheld hygrome-ter (with a detection range of 20%-99% RH), enabling pre-cise regulation of relative humidity within the chamber. The specific connection method is as follows: Connect the hu-midifier's steam outlet to a section of insulated flexible tub-ing. Pass the other end of the tubing through a pre-drilled hole in the upper side of the acrylic shell, extending it into the interior of the experimental chamber to allow moisture to diffuse naturally and evenly. Insert the humidity sensor probe into the chamber through an opening in the center of the acrylic shell to measure the relative humidity inside the chamber.

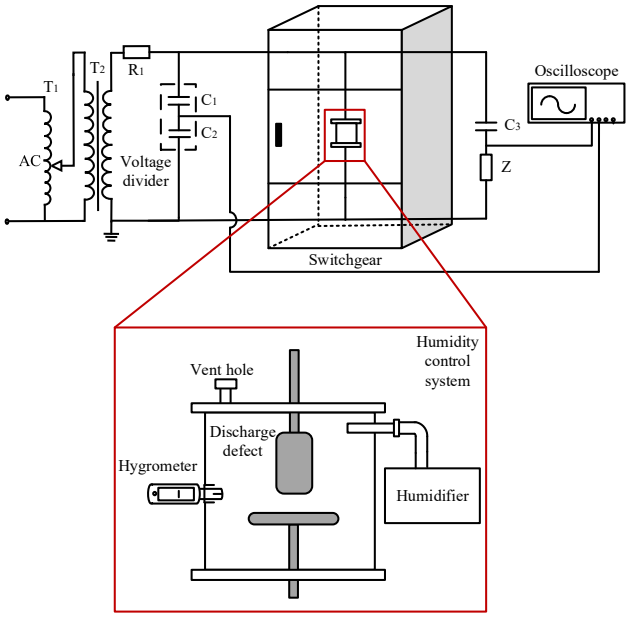

Fig. 14. Experimental Circuit Wiring Diagram

"Common Technical Requirements for High-Voltage AC Switchgear and Control Gear" (GB/T 11022-2020) [32] stipulates that the normal operating conditions for indoor switchgear require the average relative humidity measured within 24 hours not to exceed 95%, and the monthly aver-age relative humidity not to exceed 90%. To ensure experi-mental safety, all humidity adjustment operations must be completed before applying high voltage. The specific pro-cedure is as follows: Correctly install the selected defect model within the test chamber and connect the circuit. Ac-tivate the humidifier to precisely adjust the relative humidi-ty within the test apparatus to the target value. Continu-ously monitor humidity readings via the hygrometer. Once readings stabilize and remain consistent for at least 30 minutes, seal all ventilation openings of the test chamber. Shut off the humidifier and disconnect its power supply to ensure no active humidification occurs during subsequent high-voltage testing phases.

Second, PD simulation experiments were conducted. Internal air gap discharges typically occur within the epoxy resin-encapsulated bushing pillars of load switches, circuit breakers, and grounding switches. The causes of such de-fects can be attributed to two aspects: First, manufacturing process defects. During the epoxy resin casting process, in-sufficient vacuum, incomplete degassing, or improper curing techniques can leave microscopic bubbles, voids, or cracks within the insulation. Second, during actual operation, thermal expansion and contraction, electromagnetic me-chanical stresses, or prolonged exposure to minor PD itself can lead to the formation of microcracks or interfacial sep-aration within the encapsulated bushing[33]。 To simulate the aforementioned phenomenon, the internal discharge model consists of a pair of highly conductive copper column-plate electrodes and an epoxy resin insulating layer. To corre-spond to air gap defects in the simulation, the experimental air gap

defect was designed and fabricated as follows: A 10 mm diameter hollow cavity was excavated at the center of a 1 mm thick epoxy resin insulating material. A 1 mm thick epoxy resin plate was then placed on top, with another 1 mm thick epoxy resin plate positioned underneath. Finally, all three epoxy resin plates were bonded together using epoxy resin adhesive, with air serving as the medium. The surfaces and edges of the electrodes were sanded to elimi-nate burrs that could affect the test results. The distance between the two electrode plates was then precisely adjust-ed. The specifications were: flat electrodes 130 mm × 14 mm and cylindrical electrodes 30 mm × 30 mm. A sche-matic diagram of the model is shown in Figure 15.

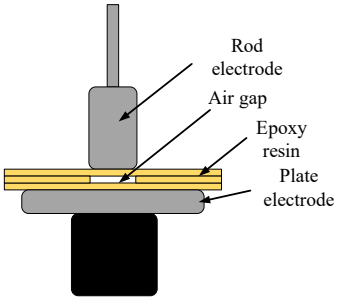

Fig. 15. Schematic Diagram of Internal Air Gap Discharge Defect Model

3.2 PD Test Validation

Prior to the test initiation, a defect-free voltage appli-cation test was conducted on the platform using the pulse current method. No partial discharge (PD) phenomena were observed within the test platform when the voltage reached 10 kV.

Subsequently, voltage application was performed on the experimental platform containing the defect model. When the voltage increased to 4 kV, a discharge signal was detected in the pulse current channel. The signal amplitude was 20 mV. With an oscilloscope sampling rate of 6.25 GS/s, the time-domain waveform of the detected PD pulse current signal is shown in Figure 16. Subsequently, continuous data was collected over one second to generate a phase-resolved partial discharge (PRPD) spectrum, as depicted in Figure 17.

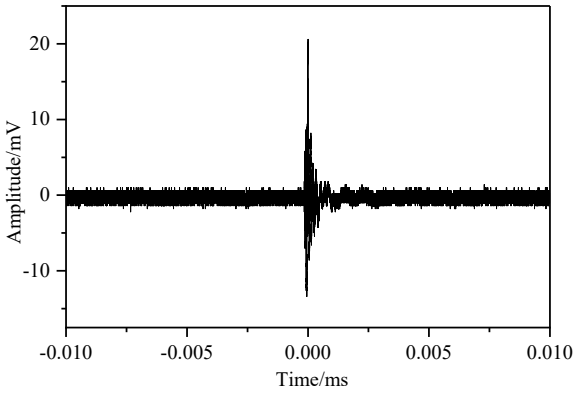

Fig. 16. Time-domain diagram of the pulse current waveform

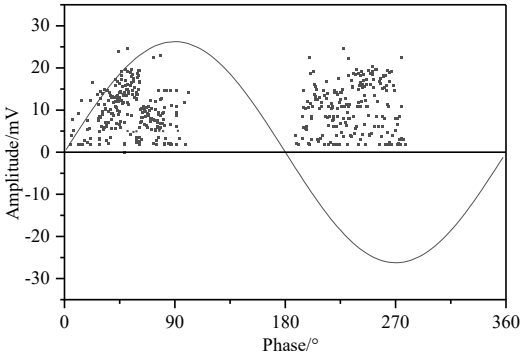

Fig. 17. PRPD Spectrum

The spectrum exhibits a typical and distinct “dou-ble-peak” structure, with discharge clusters predominantly distributed near the rising edge parts of both the positive and negative half-cycles of the power frequency voltage. This pattern demonstrates clear symmetry, characteristic of an air gap discharge spectrum. This not only aligns closely with the air gap defect model established in simulation studies but also statistically validates the effectiveness of the ex-perimental defect model.

4. Conclusion

This paper focuses on the propagation characteristics of coupled signals from discharge insulation defects in un-derground substations, establishing simulation models for both electrical signals and ground network interference sig-nal propagation. Through systematic simulation analysis and experimental verification, the following key conclusions are drawn:

1) The equivalent circuit model accurately reproduces the physical process of air gap discharge and its coupled signal characteristics. Ground network interference coupled through common ground impedance is the primary cause of degraded measurement signal-to-noise ratio. Implementing a “shared grounding point” grounding method is the key measure to sever this interference path and ensure the ef-fectiveness of capacitive insulator coupling technology.

2) The experimentally obtained PRPD spectrum, ex-hibiting a characteristic “double-peak” shape, not only aligns closely with the air gap discharge model but also demonstrates that this monitoring method achieves a leap from signal detection to defect type identification, providing scientific basis for insulation condition assessment;

3) Future research should focus on integrating mul-ti-monitoring point data and developing deep learn-ing-based intelligent diagnostic algorithms to further en-hance the system's localization accuracy and early warning capabilities.

Acknowledgments

This work was supported by the Science and Technology Project of State Grid Jiangsu Electric Power Company Limited (Grant No. J2025053).

REFERENCES

[1] T. Lakshmi, et al., "A new method for incipient fault diagnosis of power transformers based on image pro-cessing of phase resolved partial discharge pattern of transformer oil," Measurement, vol. 258, p. 119536, 2025.

[2] S. A. Belay and S. Kebede, "Investigation of groundwa-ter flow systems in the Eastern Karoo Basin along the Drakensberg Mountains to the Indian Ocean tran-sect," Journal of Hydrology: Regional Studies, vol. 62, p. 102897, 2025.

[3] S. Gath and D. Titov, "Stages of insulator wetting and drying: experimental analysis of leakage current be-haviour for flashover monitoring," Electric Power Sys-tems Research, vol. 252, p. 112417, 2025.

[4] X. Jiang, C. Zhang, Z. Zhou, et al., "Partial discharge data augmentation based on wavelet coefficients and variational autoencoder," Measurement, vol. 258, p. 119219, 2025.

[5] D. Stanković, A. Draganić, I. Orović, et al., "Detection and classification of partial discharge signals using Hermite transform and expectation-maximization ap-proach," International Journal of Electrical Power and Energy Systems, vol. 172, p. 111234, 2025.

[6] A. Abdo, L. Hongshun, L. Luyao, et al., "A novel meth-od for partial discharge source localization in three-dimensional power transformer models using par-ticle swarm optimization and particle filter-ing," Engineering Applications of Artificial Intelligence, vol. 162, p. 112566, 2025.

[7] Z T. Zhu, Y. Lin, H. Tian, et al., "A Cable Partial Dis-charge Localization Method Based on Complete En-semble Empirical Mode Decomposition with Adaptive Noise–Multiscale Permutation Entropy–Improved Wavelet Thresholding Denoising and Cross-Correlation Coefficient Filtering," Energies, vol. 18, no. 20, p. 5511, 2025.

[8] Z. Yang, Y. Wang, J. Liu, et al., "Analysis of the Influ-ence of Structural Defects on the Insulation of GIL Ba-sin Insulator Under AC Electric Field," Energies, vol. 18, no. 20, p. 5347, 2025.

[9] H. Madhuranga, K. J. W. Raymond, A. H. Illias, et al., "Robust open-set partial discharge diagnosis based on hybrid supervised contrastive learning and SVM framework," Ain Shams Engineering Journal, vol. 16, no. 12, p. 103762, 2025.

[10] Q. An, P. Li, G. An, et al., "Improved crested porcupine optimizer-VMD method applied to partial discharge signal," Measurement, vol. 258, p. 119145, 2025.

[11] K. Soni, M. Seeger, U. Straumann, et al., "Streamer pa-rameters in CO2/O2/C4F7N gas mixture for application in high voltage switchgear," Journal of Physics D: Ap-plied Physics, vol. 58, no. 44, p. 445201, 2025.

[12] X. Sun, Y. Chen, J. Wei, et al., "Switch Cabinet Temper-ature Prediction Using a Fusion of CNN and LSTM Neural Networks," Applied System Innovation, vol. 8, no. 5, p. 157, 2025.

[13] J. Heo, Y. Zhang, J. Bae, et al., "Explainable machine learning-based meta-modeling for predicting fire dam-age to motor control cabinets in a switchgear room," Nuclear Engineering and Technology, vol. 58, no. 1, p. 103862, 2025.

[14] D. Zhang, X. Yang, A. Sun, et al., "Research on Intelli-gent Condensation Recognition and Environmental State Diagnosis Method of High-Voltage Switchgear Based on STM32," Journal of Intelligence and Knowledge Engineering, vol. 3, no. 3, 2025.
[15] Q. Guo, Y. Xu, X. Zhang, et al., "Passive wireless tem-perature partial discharge integrated monitoring tech-nology for switchgear based on ultra-high frequency technology," Engineering Research Express, vol. 7, no. 3, p. 035351, 2025.
[16] A. Long, P. He, S. Wang, et al., "Fault detection of switchgear based on partial discharge gas analy-sis," Journal of Physics: Conference Series, vol. 2993, no. 1, p. 012079, 2025.
[17] Q. Zhuang, J. Zhang, J. Lin, et al., "A fault diagnosis method for partial discharge in distribution switchgear based on global Feature-enhanced residual shrinkage network," Journal of Physics: Conference Series, vol. 2935, no. 1, p. 012032, 2025.
[18] F. Liu, Z. Zhang, H. Su, et al., "Investigate and Experi-mental Verification of Early Monitoring and Warning Fire Extinguishing System for Substation Switchgear Cabinet Fire," Journal of Physics: Conference Series, vol. 3074, no. 1, p. 012029, 2025.
[19] D. Huang, S. Zhao, H. Wang, et al., "Correlation and prediction of electromagnetic disturbance characteris-tics in high voltage switchgear interrup-tions," International Journal of Electrical Power and Energy Systems, vol. 170, p. 110854, 2025.
[20] Q. Zhou, Z. Liu, Z. Jiang, et al., "High performance flexible thermoelectric generator for integrated self-powered sensors in high voltage switchgear con-tacts," Energy, vol. 334, p. 137457, 2025.
[21] R. Kindt, I. Siddique, I. Dawson, et al., "The Agroforest-ry Species Switchboard, a global resource to explore information for 107,269 plant species," Scientific Data, vol. 12, no. 1, p. 1150, 2025.
[22] H. Wu, Q. Zhang, Q. Liu, et al., "20 Seconds to fabricate high-performance NiFe-based anode for seawater elec-trolysis via bi-directional pulse current meth-od," Chemical Engineering Journal, vol. 498, p. 155435, 2024.
[23] International Electrotechnical Commission, "High-voltage test techniques - Partial discharge meas-urements," IEC 60270, 2000.
[24] State Administration for Market Regulation of the Peo-ple's Republic ofChina, Standardization Administration of the People's Republic of China. "Measurement of Partial Discharges," GB/T 7354, 2003.
[25] L. Gao, A. Zhang, and W. Lei, "Transformer Fault Di-agnosis Based on Intelligent Algorithm and Partial Dis-charge," Journal of Physics: Conference Series, vol. 2774, no. 1, p. 012039, 2024.
[26] X. Hao, B. Zhang, Z. Liu, et al., "Comparative Study on Multiple Methods for Partial Discharge Detection of Gap Defect in Medium Voltage Switchgear," Journal of Physics: Conference Series, vol. 2774, no. 1, p. 012064, 2024.
[27] R. M. R and P. M. B, "Characterization and Corrosion Resistance Behavior Study of Pure Ni Coatings and Ni–V2O5 Nanocomposite Coatings Developed by Di-rect Current and Pulse Current Methods of Electrodep-osition," Surface Engineering and Applied Electro-chemistry, vol. 59, no. 5, pp. 569-581, 2023.
[28] S. V. S, K. P. N, K. E. A, et al., "Application of Pulsed Excitation to Estimate the Corrosion Damage of Alu-minum Alloys by the Eddy Current Method," Russian Metallurgy (Metally), vol. 2022, no. 12, pp. 1518-1522, 2023.
[29] T. Xiangyu, L. Wenyun, X. Xiaowei, et al., "Contactless AC/DC Wide-Bandwidth Current Sensor Based on Composite Measurement Principle," Sensors, vol. 22, no. 20, p. 7979, 2022.
[30] R. Kindt, I. Siddique, I. Dawson, et al., "The Agroforest-ry Species Switchboard, a global resource to explore information for 107,269 plant species," Scientific Data, vol. 12, no. 1, p. 1150, 2025.
[31] M F. Mingers, S. Kimpeler, and W. Leterme, "Experi-mental characterization of evaporation processes of copper and polyamide 6.6 caused by fault arcs," Physica Scripta, vol. 100, no. 7, p. 075613, 2025.
[32] State Administration for Market Regulation of the Peo-ple's Republic ofChina, Standardization Administration of the People's Republic of China. "Common Technical Requirements for Standards of High-Voltage Switch-gear and Controlgear," GB/T 11022-2020, 2020.
[33] Wu, Q. Wang, K. Wu, et al., "Experiment on Early Fire Detection of Medium-voltage Switchgear Based on Pyrolytic Particles," Journal of Physics: Conference Se-ries, vol. 3012, no. 1, p. 012041, 2025.